JGR Oceans

RESEARCH ARTICLE
10.1029/2020JC017089

Hudson Strait Inflow: Structure and Variability

Natasha A. Ridenour[1], Fiammetta Straneo[2], James Holte[2], Yves Gratton[3], Paul G. Myers[1], and David G. Barber[4]

[1]Department of Earth and Atmospheric Sciences, University of Alberta, Edmonton, AB, Canada, [2]Scripps Institution of Oceanography, University of California San Diego, La Jolla, CA, USA, [3]Institut National de la Recherche Scientifique – Océanologie, Québec, QC, Canada, [4]Center for Earth Observation Science, University of Manitoba, Winnipeg, MB, Canada

Key Points:

- The first year-round observations of the Hudson Strait inflow shows a weakly stratified and saline flow with little seasonality
- Inflow source waters stem from the Baffin Island Current and are mainly comprised of Arctic Water
- A portion of Hudson Strait inflow flows into Hudson Bay and is transformed into Hudson Bay deep water

Correspondence to:
N. A. Ridenour,
ridenour@ualberta.ca

Citation:
Ridenour, N. A., Straneo, F., Holte, J., Gratton, Y., Myers, P. G., & Barber, D. G. (2021). Hudson Strait inflow: Structure and variability. *Journal of Geophysical Research: Oceans*, *126*, e2020JC017089. https://doi.org/10.1029/2020JC017089

Received 22 DEC 2020
Accepted 9 AUG 2021

Abstract Hudson Strait is the main pathway of heat, mass, and freshwater exchange between Hudson Bay and the Arctic and North Atlantic oceans. The outflow along the southern coast of the strait, a fresh, baroclinic jet directed toward the North Atlantic, has received more attention due to its potential impact on deep convection in the Labrador Sea. However, details about the westward, more barotropic inflow along the northern coast of Hudson Strait remain unknown due to a scarcity of observations. Hudson Strait inflow waters affect the physical and biogeochemical systems of the bay, as well as the marine ecosystem, which supports the livelihoods of many Indigenous communities surrounding the Hudson Bay region. Here, we address this knowledge gap by analyzing data from two hydrographic surveys and four moorings deployed across the strait from 2008 and 2009. Three moorings were deployed on the northern side of the strait to map the inflow, and one was deployed on the southern side of the strait to capture the outflow. Along the southern side, a stratified, fresh outflow was observed, consistent with earlier studies. Along the northern coast, the inflow is weakly stratified and more saline, with seasonal changes distributed throughout the water column. Source waters of the inflow stem mainly from Arctic Water in the Baffin Island Current. A comparison with historical data suggests that after modification in western Hudson Strait, part of the inflow enters northern Hudson Bay to become deep water in the bay.

Plain Language Summary Hudson Strait is the gateway that connects Hudson Bay to the Arctic and North Atlantic oceans. Arctic Waters (AWs) flow into the bay via Hudson Strait, mixing with other waters in the region before being exported through the strait to the North Atlantic. Waters that flow into the bay along the northern Hudson Strait coast support the ecosystem, which is a food source for the local Indigenous communities, and affects the current system within the region. We present year-long data from the northern side of Hudson Strait for the first time. On the southern coast, low salinity waters that have mixed with river waters in Hudson and James bays quickly flows out of the bay, as earlier studies have found. The current along the northern side of the strait, however, is slow, warm, and salty. Over the course of the year, wintertime cooling as well as changes in current speed occur throughout the water column. These Hudson Strait inflow waters are comprised of AWs flowing from Davis Strait. We estimate that almost half of the AW flowing south from upstream enters Hudson Strait, possibly weakening large low salinity flows that could impact the large-scale global ocean circulation.

1. Introduction

Freshwater from the Arctic Ocean enters the North Atlantic through three main gateways: Fram Strait east of Greenland, Davis Strait between Greenland and Baffin Island, and Hudson Strait south of Baffin Island (Figure 1). Waters flowing southward through Davis Strait flow into the Labrador Sea in the northwestern Atlantic, with some of this water being rerouted into Hudson Strait (Drinkwater, 1988; LeBlond et al., 1981). Hudson Strait connects the Hudson Bay Complex (HBC; including Hudson, James, and Ungava bays, Foxe Basin, and Hudson Strait) to the North Atlantic, while Fury and Hecla Strait, a narrow, shallow passage that has a small volume and freshwater flux into northern Foxe Basin (Barber, 1965; Ridenour et al., 2019; Sadler, 1982), connects the HBC to the Arctic Ocean via the Canadian Arctic Archipelago. Hudson Strait has water flowing into the HBC from the Baffin Island Current (BIC), via Davis Strait, along its northern coast and outflowing water from the HBC along its southern coast (Drinkwater, 1988; LeBlond et al., 1981).

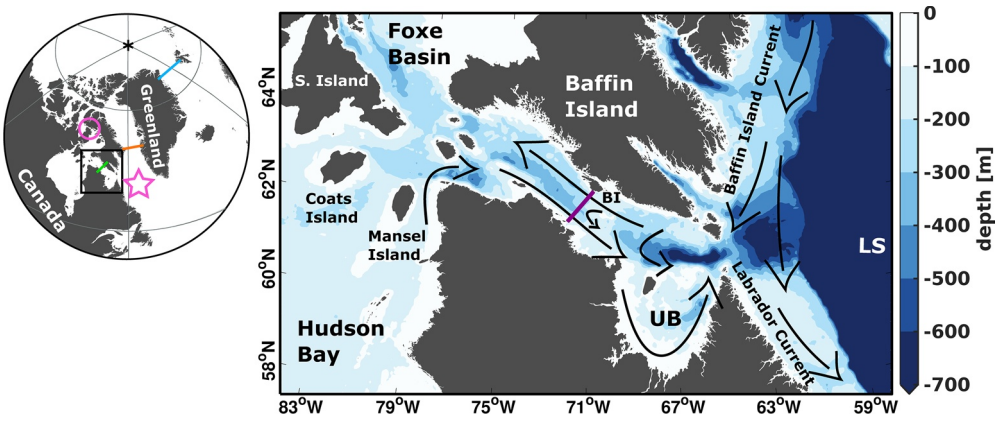

Figure 1. Bathymetry of Hudson Strait with known circulation shown. The circular map shows the location of the strait (indicated by the black box) and its proximity to the Labrador Sea and its deep convection site indicated by the star, as well as Fury and Hecla Strait, indicated by the pink circle. The blue, orange, and green bars indicate Fram, Davis, and Hudson straits. Other geographical features include S. Island (Southampton Island), BI (Big Island), UB (Ungava Bay), and LS (Labrador Sea). The purple bar indicates the location where data used in this study were collected.

The Hudson Strait outflow feeds the inshore portion of the Labrador Current (Florindo-López et al., 2020), which flows along the western Labrador Sea, and provides the Labrador Current, which has a freshwater flux of 180 mSv (using a reference salinity, S_{ref}, of 34.8), with half of its freshwater (Loder et al., 1998; Straneo & Saucier, 2008b). A third of this freshwater is derived from river input into the HBC, as nearly 900 km^3/year (29 mSv) of river discharge enters the HBC (Déry et al., 2005; Ridenour et al., 2019), draining over a third of the Canadian land area. The Hudson Strait outflow, combined with increased freshwater transport to the North Atlantic from melting Arctic sea ice, increased discharge from Greenland, and an intensified hydrological cycle (Bamber et al., 2018; Haine et al., 2015) could potentially impact deep convection sites in the North Atlantic, which play an important role in the Atlantic Meridional Overturning Circulation (Bakker et al., 2016; Böning et al., 2016; Lazier, 1980; Yang et al., 2016).

Hudson Strait inflow waters on the northern side of the strait, stemming from the BIC, are the largest source of oceanic water to the HBC (Drinkwater, 1988; LeBlond et al., 1981; Ridenour et al., 2019; Straneo & Saucier, 2008b). The HBC is a marginal sea that receives a large volume of continental runoff and freezes over seasonally due to the influence of polar air masses (Candlish et al., 2019). This area is home to over 40,000 people, and the oceanography of the HBC is relevant to their communities for trade, transport, as well as cultural and social practices (Babb et al., 2019). Additionally, the main route for the shipping industry, which transports goods from the Canadian Prairies and natural resources from local mines, is through Hudson Strait (Babb et al., 2019). Most of these cultural and economic activities revolve around the seasonal ice cover in the region, which is experiencing earlier melt and later freeze-up (Castro de la Guardia et al., 2017; Hochheim & Barber, 2014). Therefore, a knowledge of the water masses entering the HBC is key to understanding the transformations that occur within the bay and, eventually, of any variability associated with external forcings.

Hudson Strait is about 100 km wide and 400 km long, oriented northwest-southeast (Figure 1). Northwestern Hudson Strait is connected to Foxe Basin in the north and Hudson Bay to the south. Depths in this region are 200–300 m. Depths reach 900 m in the eastern Hudson Strait where it connects to the Labrador Sea. Eastern Hudson Strait is under greater influence from the Labrador Sea, with warmer and more saline waters, while in western Hudson Strait, waters are cooler and fresher (Drinkwater, 1988).

Our present understanding of flow through Hudson Strait is based on mooring deployments near the southern side of the strait from 2004 to 2006, as well as an 8 week deployment (mid-August to mid-October) in 1982 that sought to capture the flow across the whole strait (Drinkwater, 1988; Straneo & Saucier, 2008b; Sutherland et al., 2011).

The fresh, baroclinic, eastward outflow along the southern side of Hudson Strait is strongly stratified year round and influenced by the riverine waters from Hudson and James bays. Minimum salinity occurs between October and December, with maximum salinity from March to May (Straneo & Saucier, 2008b). Flow is directed along the strait, with the largest velocities at the surface during autumn (Straneo & Saucier, 2008b).

In contrast, year-long measurements of the inflow on the northern side of the strait (Hudson Strait inflow, hereafter) have yet to be presented. Limited moored data suggests that the inflow is barotropic, homogeneous, and possibly a continuation of the BIC (Drinkwater, 1988). Upstream of Hudson Strait, around 63°N, the BIC separates into two branches. The western branch enters Hudson Strait, while the eastern branch flows southward to join the Hudson Strait outflow in the inshore branch of the Labrador Current south of Hudson Strait (LeBlond et al., 1981). Previous studies have speculated that waters from Baffin Bay travel through Davis Strait to form the Hudson Strait inflow (Drinkwater, 1986, 1988; Florindo-López et al., 2020; Jones & Anderson, 1994; Straneo & Saucier, 2008b); other studies have suggested that modified deep Labrador Sea water contributes to the inflow (Jones & Anderson, 1994). However, without observations this is difficult to determine. Volume transport in the inflow is estimated to be 0.82–0.84 Sv, with a freshwater transport of 41 mSv ($S_{ref} = 34.8$; Drinkwater, 1988; Straneo & Saucier, 2008a). Straneo and Saucier (2008b) speculate that about 25% of the Davis Strait volume flux and 35% of its freshwater goes into Hudson Strait.

The fate of the inflowing waters in the HBC is similarly unknown. Earlier studies have suggested that Hudson Strait inflow waters flow either solely into Hudson Bay, west of Mansel Island, or flow into both Foxe Basin (at depth) and Hudson Bay (Defossez et al., 2012; Florindo-López et al., 2020; Jones & Anderson, 1994). Current reversals at middepth in northeastern Hudson Bay have been noted in both observational and model data, which suggests that waters from Hudson Strait can enter the bay between Mansel Island and Quebec (Granskog et al., 2011; Prinsenberg, 1986a; F. J. Saucier et al., 2004; St-Laurent et al., 2012; Tao & Myers, 2021) as well as between Mansel and Coats islands (F. Saucier et al., 1994; Tao & Myers, 2021).

In this study, we present the first year-round observations of the Hudson Strait inflow to describe its structure and its variability. Furthermore, through a comparison with existing hydrographic data, we investigate the source waters for the inflow and the pathways into the HBC. Section 2 describes the mooring set up and data processing, followed by an in-depth look at the properties of both the inflow and outflow using data collected by the hydrographic surveys and moorings (Sections 3 and 4). Source waters and inflow pathways are presented in Sections 5 and 6, respectively. We discuss our findings and future work in Section 7.

2. Data

Hydrographic sections were occupied during cruises for mooring deployment and recovery on August 26, 2008 and September 25–26, 2009 respectively. The location of the transects are shown in Figure 2, along with mooring locations and other geographic features.

Four moorings were deployed across Hudson Strait between Big Island and Wales Island (Figure 2) from August 2008 to September 2009 (the data set was published by Straneo, 2014) to map the seasonal variability in properties and transports across the strait. Mooring A was deployed on the slope of the southern coast, to capture the center of the outflow, 23 km from Wales Island, while three moorings (E, F, and G) were deployed on the northern side of the strait, located 32, 19, and 7 km from Big Island. We assume that the flow between Big Island and Baffin Island, as well as between Wales Island and Quebec, is negligible, as the passages are shallow and narrow. The moorings are located along the same transect used by Straneo and Saucier (2008b) and Sutherland et al. (2011).

2.1. Instrumentation

Instrumentation on the four moorings is summarized in Table 1 and instrument locations are shown in Figure 3d. Mooring A, on the southern coast, was deployed on the slope (Figure 3d), and was equipped with four Seabird MicroCAT CTDs (Conductivity, Temperature, and Depth) providing temperature, salinity, and pressure, two temperature sensors (HOBO UTBI-001 TidbiTs), and an upward looking RDI Acoustic Doppler Current Profiler (ADCP). The ADCP was programmed to sample the velocity every hour for the depth range 18–138 m, with 10 m bins, 30 pings per ensemble, and a short-term error of 1% of the water velocity

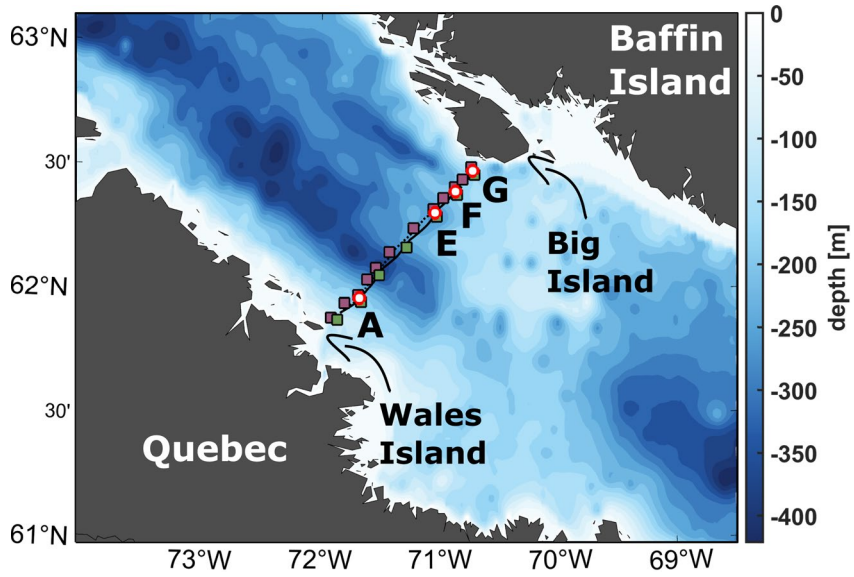

Figure 2. Mooring and hydrographic data location. The 2008 and 2009 ship transects are shown in solid and dashed lines respectively, while four mooring locations are indicated with red and white circles and their associated name. Squares indicate locations of CTD casts for 2008 (green) and 2009 (purple).

and a long-term error (bias) of 2.5 cm s^{-1}. The MicroCAT at 25 m was mounted below a 5.8 m flotation aluminum tube meant to sustain hits by icebergs or ice ridges. Blow down of this tube by the current was pronounced but allowed for data to be acquired at such shallow depths.

Table 1
Instrumentation on Moorings A, E, F, and G in Hudson Strait

	A	E	F	G
Latitude [°N]	61.9792	62.3237	62.4087	62.4913
Longitude [°W]	−71.6570	−70.9999	−70.8217	−70.6710
Bottom depth [m]	186	345	357	345
T,S sampling				
MicroCATS (15 min)	25 m (CTD), 45 m (CTD), 100 m (CT), 160 m (CTD)	40 m (CTD), 120 m (CT)	25 m (CTD), 45 m (CTD), 80 m (CT), 320 m (CTD)	40 m (CTD), 120 m (CT)
TidbiTs (15 min)	75 m (T), 135 m (T)	80 m (T), 150 m (T)	150 m (T), 180 m (T), 230 m (T), 270 m (T)	
RBR CTD (15 min)		190 m (T)		200 m (CTD)
U,V sampling				
ADCP (1 h)				
Long Ranger 75 kHz	160 m (CTD)[a]			
Workhorse 300 kHz			80 m (CTD)[b]	
Current meter (20 min)				
Nortek Aquadopp		300 m (TD)[c]		300 m (TD)[d]
Ice sampling (ULS)	45 m		45 m	

Note. Geographic location of the moorings and depths of the instruments are shown, with sampling intervals for each instrument in parentheses. The MicroCATS used were all Seabird SBE MicroCATS, while TidbiTs were all HOBO UTBI-001 TidbiTs. Instruments that sampled salinity, temperature, or pressure are indicated with C, T, or D respectively. The two ADCPs used were RDI ADCPs. Time periods of data obtained from current meters and ADCPs are shown in the footnotes in day/month/year format.
[a]26/08/2008 to 24/09/2009. [b]27/08/2008 to 04/03/2009. [c]26/08/2008 to 24/09/2009. [d]25/08/2008 to 24/09/2009.

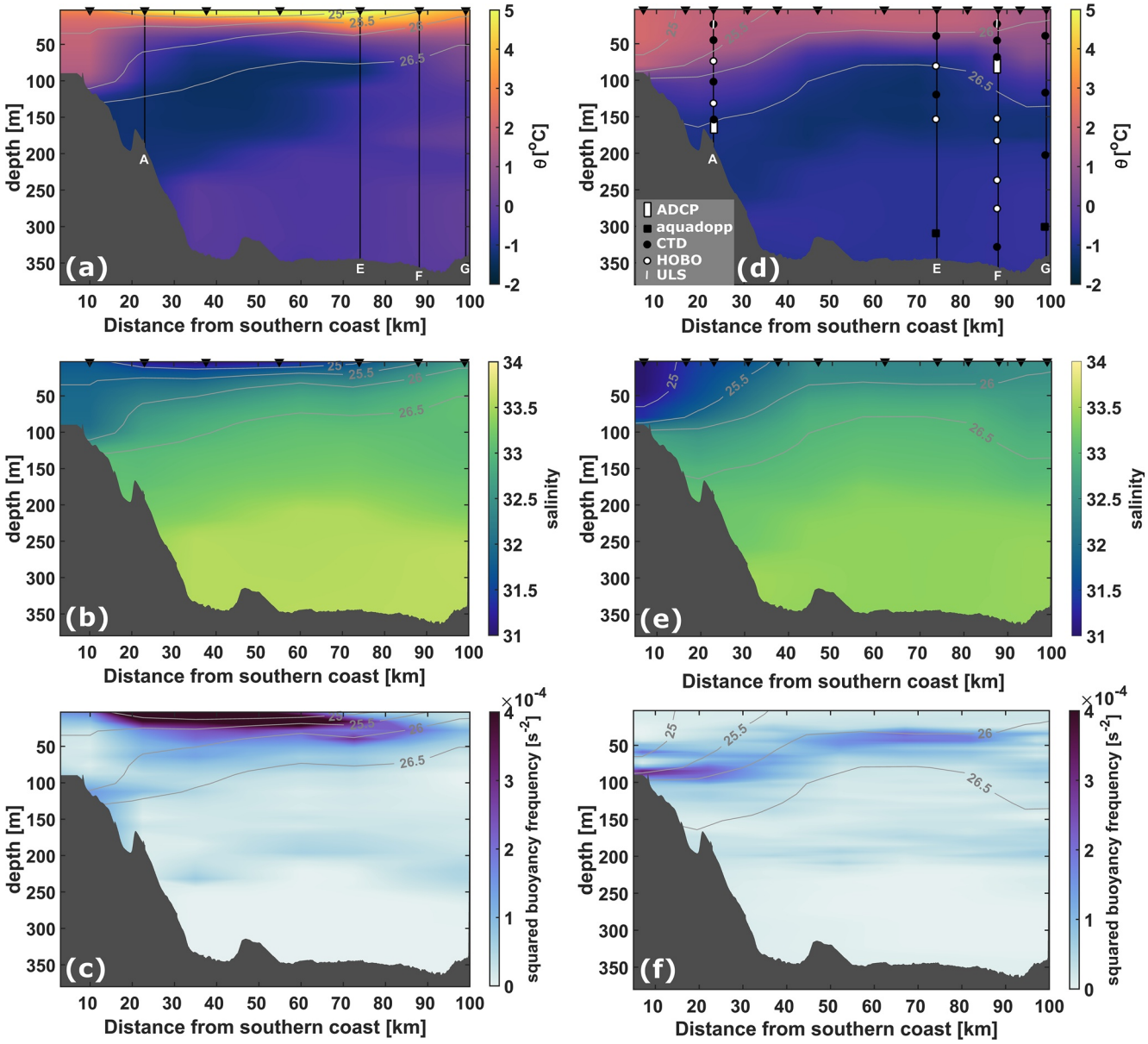

Figure 3. Potential temperature (a, d), practical salinity (referred to as salinity, hereafter) (b, e), and squared buoyancy (Brunt-Väisälä) frequency ($N^2 = -\frac{g}{\rho_o}\frac{d\rho}{dz}$) (c, f) for the August 2008 hydrographic section taken upon mooring deployment (left) and the September 2009 hydrographic section (right) taken upon mooring recovery. Isopycnals (σ_θ) are overlaid on all panels. Black triangles in panels (a–d) indicate the CTD (Conductivity, Temperature, and Depth) cast locations. Mooring set up is shown in panel (d), including ADPCs (Acoustic Doppler Current Profiler), aquadopps, CTD, HOBO TidbiTs (indicated as HOBO here), and two Upward Looking Sonars (ULS).

Mooring E was positioned to capture the outer edge of the inflow on the northern side of the strait. The mooring was equipped with a Nortek Aquadopp current meter at 300 m, two Seabird MicroCAT CTDs, and two temperature sensors (TidbiTs). The northern most mooring, Mooring G (depth 345 m), was set up similarly to Mooring E.

To capture the center of the inflow, Mooring F had a MicroCAT mounted to the bottom of an aluminum tube at 25 m as on Mooring A. An RDI ADCP was located at 80 m, capturing flow every hour between 7 and 67 m, with a 4 m bin size and 120 pings per ensemble. The short-term error of the ADCP on Mooring F was 0.5% the water velocity, with a long term error of 2.5 cm s^{-1}. Unfortunately, the battery of this ADCP

was depleted by March 4, 2009. A second ADCP was positioned on the mooring at 320 m, however, it failed immediately. We note that the two Upward Looking Sonars (ULS) on Moorings A and F were not analyzed in this study.

Bathymetry in spatial plots is from the ETOPO1: Earth Topography and Bathymetry data set (ETOPO1 1 Arc-Minute Global Relief Model, 2009; Amante & Eakins, 2009). Bathymetry shown in cross-section plots is from the Knudsen 12 and 3.5 kHz chirp sonar aboard the RV Knorr. We note that there are discrepancies between the two data sets, indicating the need for further bathymetric mapping in the strait.

2.2. Calibration and Post-Processing

All moored CTD recording instruments were factory calibrated prior to deployment and potential drifts in conductivity and temperature were investigated through comparison with the ship's CTD data. Cross-calibration with nearby instruments was similarly used to identify potential drifts in temperature, conductivity, and pressure. The processing procedure is described in detail by Ramsey and Straneo (2018).

The ADCP data were quality controlled by removing all data points with error velocities larger than 0.25 m s^{-1}; overall this amounted to less than 2% of data at all moorings. These data gaps were filled by interpolating in the vertical. About 8% of the data were lost to sidelobe interference which resulted in no data over the upper 15 m at A and 5 m at F. The depth of the transducer was obtained by deriving a corrected sound speed, at the transducer depth, from the MicroCATs co-located with the ADCPs. The same correction was used to derive the depth array for the bins (Ramsey & Straneo, 2018). The magnetic declination was applied to the velocity data from the 11^{th} generation International Geomagnetic Reference Field model, released in December 2009 (Finlay et al., 2010).

Potential temperature and salinity data were linearly interpolated in the vertical and binned into daily and monthly averages. Velocities included in our analysis were from two ADCPs (Moorings A and F) and two Aquadopps (Moorings E and G). Velocities were rotated 33.4° into along- and cross-strait directions; this was determined by principal component analysis (88% and 11% explained). Velocities were detided with the Matlab t-tide package (Foreman et al., 1998; Pawlowicz et al., 2002) before being analyzed.

2.3. Additional Temperature and Salinity Data

To determine source waters and inflow pathways, we supplemented our data with temperature and salinity data from both east and west of Hudson Strait from the World Ocean Database (Boyer et al., 2018) and the Oceanography and Scientific Data-Marine Environmental Data Service (http://www.meds-sdmm.dfo-mpo.gc.ca/). Data from the BIC was limited to August and September 2008 and 2009, at depths shallower than 400 m, consistent with the time period of the measurements described here. Data located inside the HBC was limited to the years 2000–2010 (August–October), as there was not enough data to limit to 2008 and 2009.

2.4. Additional Sea Ice Concentration Data

We also used daily 6.25 km resolution AMSR-E sea ice concentration data (Spreen et al., 2008) to provide sea ice conditions at the moorings. The grid points nearest to each mooring are used to represent the sea ice concentration.

3. Hydrographic Section Analysis

3.1. Temperature and Salinity

The hydrographic sections shown in Figure 3 were gridded and then extrapolated horizontally (invariant) using the nearest cast to the coast. These sections show the main features noted in earlier studies (Drinkwater, 1988; Straneo & Saucier, 2008a), notably, the strongly stratified surface layer, warm and saline waters at depth, and cold temperatures (below −1°C and associated with salinities of 33) at mid-depth along the

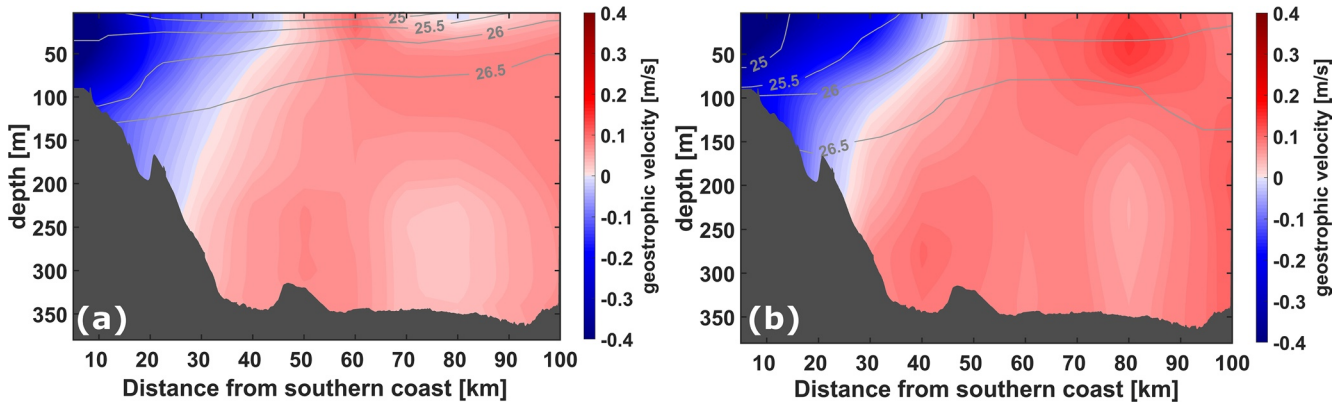

Figure 4. Calculated geostrophic velocities for hydrographic sections in (a) 2008 and (b) 2009. Isopycnals (σ_θ) are overlaid on both panels. Both sections are referenced at 100 m to observed velocities and assume 0.1 Sv transport out of the strait. Positive values (red) indicate inflowing waters toward the HBC, while negative values (blue) show outflowing waters away from the HBC and toward the Labrador Sea.

southern coast. The location of the lowest salinities along the southern coast is also consistent with previous work (Drinkwater, 1988; Straneo & Saucier, 2008a). Higher salinities and cooler temperatures, in addition to weaker stratification, are present along the northern coast, in agreement with previous work (Drinkwater, 1988; Straneo & Saucier, 2008a).

Differences, however, do exist between the two section occupations. The maximum stratification was located along the 1,026 kg m^{-3} isopycnal in September 2009, whereas in August 2008, the maximum stratification was at the surface. The lowest salinity waters in August 2008 were offshore at the surface, whereas in September 2009 they remained along the southern coast in the boundary current, in agreement with earlier studies. The cold, mid-depth layer was present in both sections, but extended across the whole strait in September 2009. Finally, near the bottom of the strait, warmer and more saline waters were present in August 2008. The inflow was cooler and less saline in September 2009 compared to August 2008.

3.2. Geostrophic Velocities and Transports

Absolute geostrophic velocities for each hydrographic section (August 26, 2008 and September 25–26, 2009) were obtained by calculating the geostrophic stream function. The geostrophic velocities were referenced to 100 m velocities observed by moored instruments. We note that there is uncertainty with the reference velocities, and our choice was based on what seemed to be the most reasonable solution while still acknowledging the uncertainty. To determine the reference velocity, bottom velocities at Mooring F were interpolated using the measured bottom velocities at Moorings E and G. The Mooring F velocity at 100 m was then interpolated using the observed near-surface velocities and the interpolated bottom velocity. To obtain 100 m velocity values at Moorings E and G, we assume the flow at Mooring F is homogeneous across the northern side of the strait, and interpolated the 100 m value using the surface velocities at F and the bottom velocities at Moorings E and G respectively. As the ADCP on Mooring F failed in March 2009, 2008 velocities were used to obtain a 100 m reference velocity in September 2009 at Mooring F. Geostrophic velocities were then adjusted for −0.1 Sv net transport through the strait (Figure 4; see Appendix A for more details), which is an approximate estimate by Drinkwater (1988) from an 8 week mooring deployment in the 1980s. The caveat, aside from the short time series, being the estimated annual net volume transport of −0.1 Sv is not the same as a snap-shot of net transport in time, as this would change during the year and interannually.

The uncertainty in the 2008 geostrophic velocities, determined by Monte Carlo analysis by randomly removing 30% of the data over many iterations, was 0.05 m s^{-1} (the standard deviation), while the uncertainty in the 2009 calculated geostrophic velocities was 0.03 m s^{-1}. The geostrophic velocities showed a strong outflow along the southern coast. The largest outflow velocities were located closest to the coast, and decreased northwards. The width of the outflow was about 45 km in both sections. The inflow structure, on the other hand, was broad, with weaker velocities throughout the water column, consistent with Drinkwater (1988). In August 2008, weak inflow velocities were observed at the surface, including a small flow reversal 20 km

Table 2
Volume, Freshwater, Salt, and Heat Transports for Two Hydrographic Sections

	August 2008	September 2009
Net volume	−0.1 Sv	−0.1 Sv
Inflow	2.0 Sv	2.8 Sv
Outflow	−2.1 Sv	−2.9 Sv
Net freshwater	−54 (−56) mSv	−69 (−71) mSv
Inflow	−14 (90) mSv	−10 (135) mSv
Outflow	−40 (−146) mSv	−59 (−206) mSv
Net salt	−2 kt/s	−1 kt/s
Inflow	68 kt/s	95 kt/s
Outflow	−70 kt/s	−96 kt/s
Net heat	−8.1 TW	−9.2 TW
Inflow	−0.5 TW	−6.3 TW
Outflow	−7.6 TW	−2.9 TW

Note. Salt transport is in units of kilotonnes per second. Freshwater is referenced to a salinity of 33 (34.8) while heat transports are referenced to a temperature of 0°C. Negative values indicate a flux out of the HBC.

from the northern coast. Weak velocities were present below 150 m depth. Comparatively, the 2009 section contained larger inflow velocities throughout the section, including a subsurface maximum 20 km from the northern coast.

Presently, it is unknown if the inflow is impacted by the sill (approximately 110 m depth) to the east of the mooring array on the northern side of the strait (Figure 2).

Net volume transports for August 2008 were smaller overall compared to September 2009 (Table 2). Transports derived from these synoptic sections were larger than the mean, year-round transports estimated by Straneo and Saucier (2008a). Net heat and salt transports were similar in both sections. The net salt transport in the strait was nearly zero for both August 2008 and September 2009 (as it is a salt budget, no reference salinity was used). Overall, a net export of freshwater occurs through Hudson Strait, with the relative contributions of the inflow and outflow being sensitive to the chosen reference salinity. The transport-weighted (practical) salinity (TWS) for the outflow was 32.38 in 2008, and 32.33 in 2009 (August and September respectively). Inflowing waters were more saline, with TWS values of 33.24 in August 2008 and 33.12 in September 2009. We also calculated the transport-weighted temperature (TWT) for both the inflow and outflow, as the heat transport appears to vary with the properties in the inflow as well as the position and extent of the cold intermediate layer (CIL). These values were for August and September respectively, and are likely to change throughout the year. In 2008, the TWT for the inflow was −0.06°C, while the outflow was 0.97°C. Comparatively, in 2009 the outflow had a TWT of 0.21°C, while the inflow was −0.54°C.

In both years, fresh waters flow toward the Labrador Sea and more saline waters flow into Hudson Strait (Figure 5). In September 2009, the fastest outflowing velocities were associated with the warmest and freshest waters. September 2009 also showed a reduced range in both temperature and salinity compared to August 2008.

4. Moored Data Analysis: Overview of Hudson Strait Inflow and Outflow

4.1. Temperature and Salinity

4.1.1. Outflow

Our data on the southern side of the strait shows similar features to observations presented earlier by Drinkwater (1988), Straneo and Saucier (2008b, 2008a), and Sutherland et al. (2011), though our data also shows some variability in the timing of seasonal signals. Below, we discuss a few differences between the data sets.

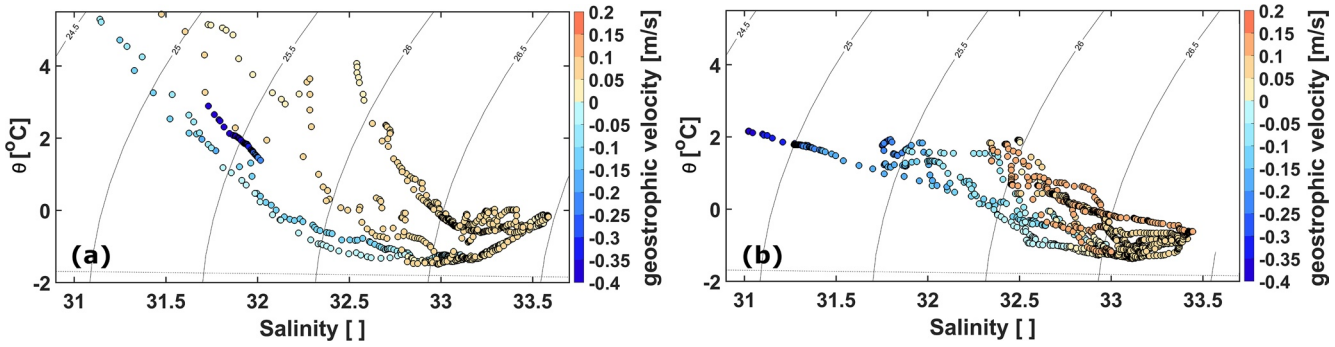

Figure 5. Potential temperature-salinity plot with associated geostrophic velocities for (a) the 2008 hydrographic section and (b) the 2009 hydrographic section.

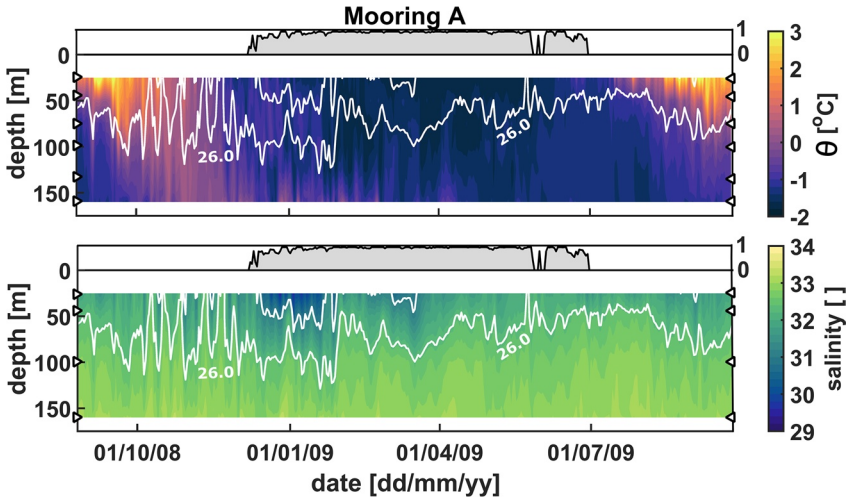

Figure 6. Mooring A potential temperature (top) and salinity (bottom) for the mooring deployment period. Data shown are in daily averaged bins. Depths where discrete measurements were taken are shown by the black and white triangles. Linear interpolation was used at depths where instruments were not present. White lines denote isopycnals (σ_θ) at 25.0 and 26.0 (only 26.0 is labeled). Sea ice concentration (in gray) from daily AMSR-E data is also shown for the mooring deployment period with its axis on the right-hand side.

The salinity dropped below 31 twice in our observations (Figure 6, bottom panel). The first instance occurred in December 2008 to January 2009, indicating the passing of the spring freshet from Hudson and James bays earlier in the year, and occurred at the same time as the arrival of sea ice. The waters from the spring freshet flow along the eastern coast of Hudson Bay and remain along the coast as the flow enters Hudson Strait (Déry et al., 2005; St-Laurent et al., 2011; Straneo & Saucier, 2008b). The second instance occurred in March 2009. This second pulse did not appear in Straneo and Saucier (2008b)'s observations, potentially because their shallowest measurements were at 55 m. The pulse was not clearly discernible at the 100 m MicroCAT in our data, implying that it was an event contained in the top 50 m. With regards to high frequency variability, individual low salinity events (anticyclonic eddies) were identified from October to April in the data presented by Sutherland et al. (2011). In our data set, however, we found low salinity events from September to November, but during the passing of the spring freshet, identifying individual events was more difficult. These low salinity events might also be similar to those described by Marsden and Gratton (1998).

We use transport-weighted means to provide a more complete picture of the properties of the flow. The fastest velocities are associated with the lowest salinities in the outflow, and therefore should be weighted more than waters with slower velocities. Using transport-weighted means also makes the properties more comparable to earlier papers. The transport-weighted mean temperature at Mooring A was −0.72°C (28–138 m) for the mooring deployment time period. This estimate was close to the two transport-weighted estimates of −0.75°C (empirical estimate, based on the relationship between Moorings A and B) and −0.91°C (dynamical estimate, based on geostrophy) for Mooring A in Straneo and Saucier (2008b). The transport-weighted mean salinity for the outflow was 32.13, which is higher than the transport-weighted values of 31.93 (empirical) and 31.59 (dynamical) by Straneo and Saucier (2008b).

4.1.2. Inflow

The data from the three moorings on the northern side of the strait are the first year-round measurements of the properties of the inflow (Figure 7). All three inflow moorings showed seasonal heating at the surface during the summer months, and cold temperatures that extended from the surface to at least 200 m depth in winter. Cold mid-depth waters on the northern side of the strait laid between −1°C and 0°C, and were only present at the beginning of the time series.

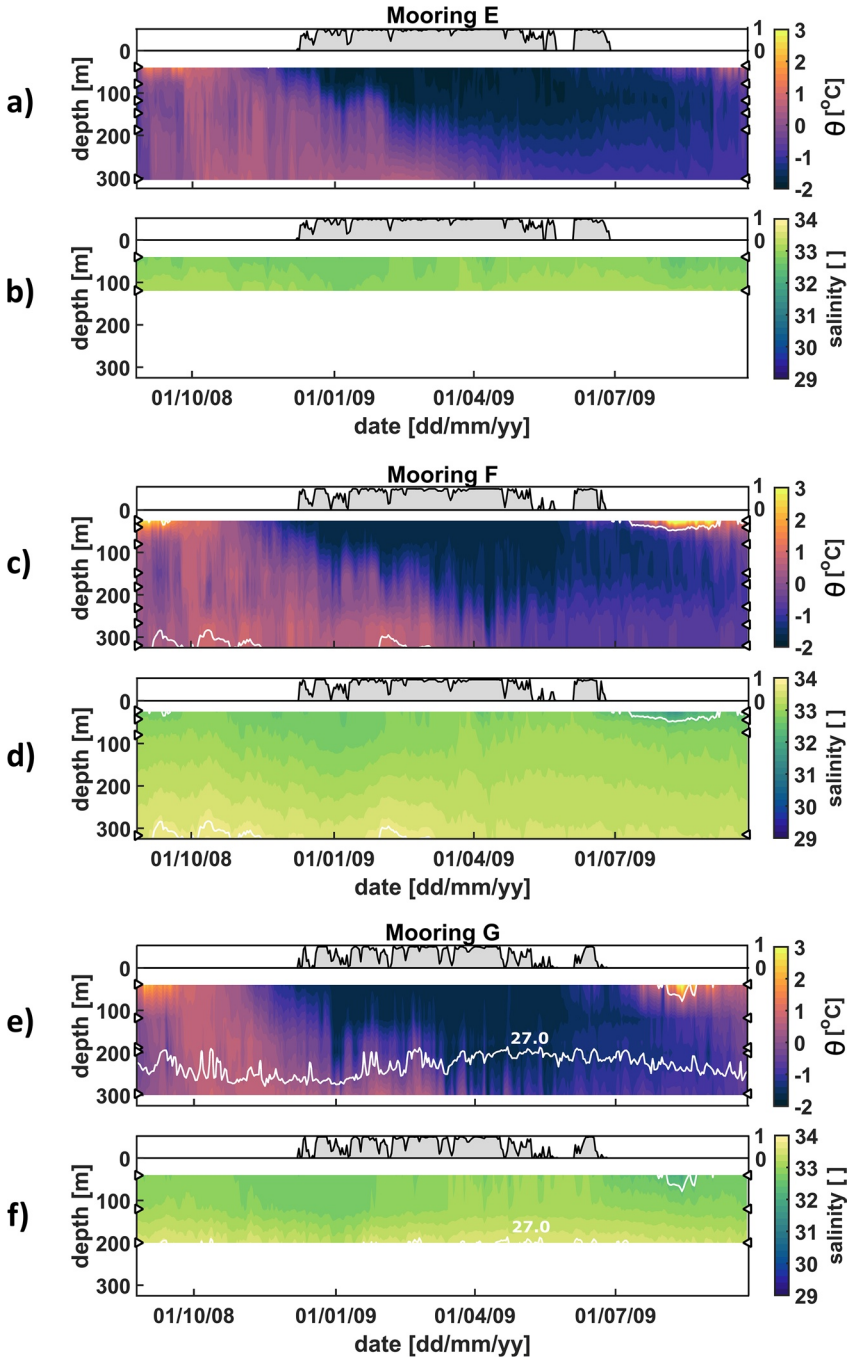

Figure 7. Potential temperature and salinity data for the mooring deployment period for Moorings E (a, b), F (c, d), and G (e, f). Temperature panels are (a, c, and e), while salinity panels are (b, d, and f). Data shown are in daily averaged bins. Locations where discrete measurements were taken are shown by the black and white triangles. White lines denote isopycnals (σ_θ) at 26.0 and 27.0 (only 27.0 is labeled). Sea ice concentration from daily AMSR-E data is also shown for the mooring deployment period with its axis on the right-hand side.

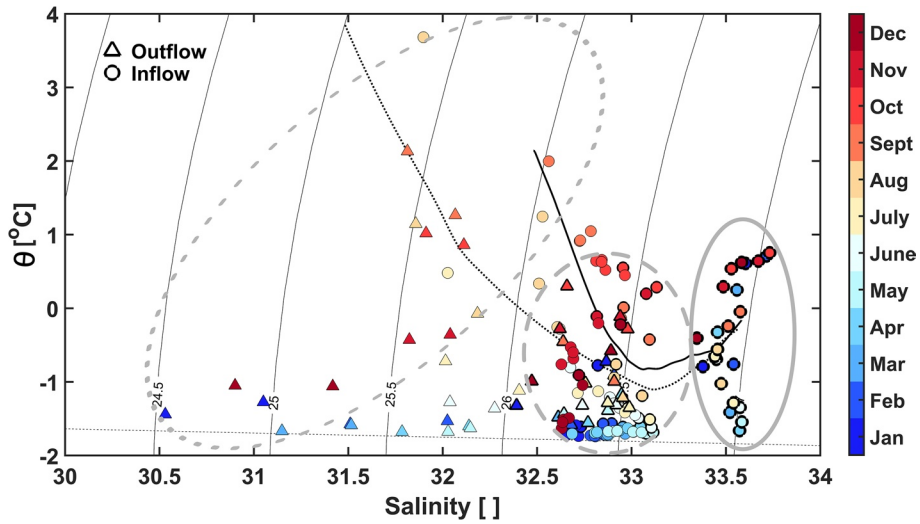

Figure 8. Monthly averaged potential temperature and salinity properties for each instrument in the mooring array. Circles show data from Moorings E, F, and G, while triangles show data from Mooring A. The outline of each shape specifies a depth range, where thin outlines show waters 0–99 m, medium outlines show waters from 100 to 199 m, and thick outlines show waters 200 m to the bottom. The dotted and solid black lines show a smoothed mean outflow and inflow profile respectively from the 2008 and 2009 CTD data. The thin dotted line indicates the freezing line. Finally, gray ellipses indicate the three classes of water observed in the strait (see text for details).

Differences between the inflow moorings were also present. Warmer surface waters (presumably due to summer heating) extended over a thinner layer at Mooring E compared to F and G, while cold winter temperatures below −1°C did not penetrate as deep at Mooring F than at Moorings E and G.

Inflow salinities generally laid between 32 and 33.8, and occasionally dropped below 32 at the surface (Figures 7d and 7f in summer 2009). The 33 isohaline hovered around 100 m depth during the majority of the year at all three moorings except Mooring G from March–June 2009 (Figure 7f).

To obtain transport-weighted mean property estimates for the inflow, the velocity observations from Mooring F were extended to 320 m using an adjusted geostrophic velocity profile from the hydrographic data. The transport-weighted averages reflect a time period of August 27, 2008 to March 4, 2009, over 30–320 m. We found a transport-weighted mean inflow temperature of −0.10°C and a transport-weighted mean inflow salinity of 33.12.

4.1.3. Comparison of the Inflow and Outflow

One major difference between the flows on the northern and southern sides of the strait, is the reduced seasonal variability in the inflow compared to the outflow. This is consistent with the absence of the seasonal freshwater export from the HBC on the northern side of the strait.

Based on data from the hydrographic section and the moorings, the water masses flowing through Hudson Strait can be separated into three broad classes (Figure 8). The first are surface waters, which are subject to modification by seasonal air-sea fluxes and riverine input, and have different properties on the southern (outflow) and northern (inflow) sides of the strait. The second class contains the CIL (Cyr et al., 2011; Petrie et al., 1988), with salinities between 32.5 and 33. These waters are present in both the inflow and outflow. The final class includes the warm, saline bottom waters, which are only present in the inflow.

Figure 8 also highlights the differences between the two flows. Inflowing waters tend to be both more saline and dense than their outflowing counterparts. Outflowing waters do not reach salinities greater than 33 (Figure 8). A migration of properties toward the freezing point line is also visible from December to June while, from July to November, waters are warm and away from the freezing point.

Cold intermediate waters from June to October are from the previous winter and gives Hudson Strait data a "hockey stick" shape during these months (Figure 8 dotted and solid black lines). The CIL is locally formed

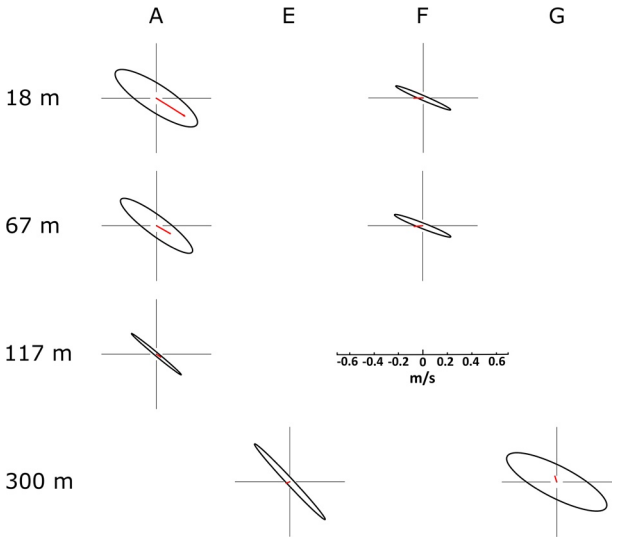

Figure 9. Tidal ellipses of the M2 tide for the moorings at four depths. Black lines for each ellipse are drawn from ± 0.05–0.45 m s^{-1}. Red arrows in each diagram show the mean residual flow for the velocity data available at that depth.

in Hudson Strait (Figure 7); however, cold intermediate waters formed upstream of both the inflow (BIC) and outflow (Hudson and James bays, as well as Foxe Basin) would also be advected through the mooring array.

4.2. Velocities in Hudson Strait

4.2.1. Tides

Tides in Hudson Strait are some of the largest in the world, with a total tidal range of 3 to over 10 m (Arbic et al., 2007; O'Reilly et al., 2005). During the mooring deployment cruise, the tidal range near Big Island was 12 m, while across the strait, near Wales Island, the tidal range was 10 m. The associated tidal currents can reach up to 1 m s^{-1} (Drinkwater, 1986). Tides are predominantly semidiurnal in Hudson Strait, with the M2 constituent being the largest, followed by S2. The M2 constituent accounted for 28%–40% of the tidal current signal in our data set, followed by the S2 constituent, ranging from 8%–13%. Tidal ellipses for the M2 tide from the mooring data are shown in Figure 9. The velocities in Hudson Strait are dominated by tides, especially at depth (Figure 9). The orientation of the ellipses indicate that the tidal current flow is along the strait. Mooring A shows reduced tidal velocity with depth, indicating baroclinic tides, whereas tides at Mooring F are uniform over the layers observed. The tidal currents at Moorings E and G are larger at depth (below sill depth) than at the surface, suggesting a modification due to topography.

The sill seaward of our mooring line is likely to give rise to substantial mixing given the strong tidal currents. Further surveys and analysis will be needed to determine the impact this sill has on the water properties flowing into and out of the strait at the mooring line.

4.2.2. Velocities in the Inflow and Outflow

The residual mean flows, obtained after the removal of tides, are shown in Figure 10. The outflow field on the southern side of the strait (Figure 10) is directed along-strait and shows many of the features described by Drinkwater (1988) and Straneo and Saucier (2008b). The seasonality of the outflow velocity is strongest near the surface, with the fastest surface velocities coinciding with the lowest salinity surface waters.

On the northern side of the strait, data are more limited due to the failure of the deep ADCP on Mooring F and the battery failure of the shallow ADCP on Mooring F, only providing us with six months of data. Thus our description of the flow field focuses on the six months of available data we have, covering 7–67 m depth.

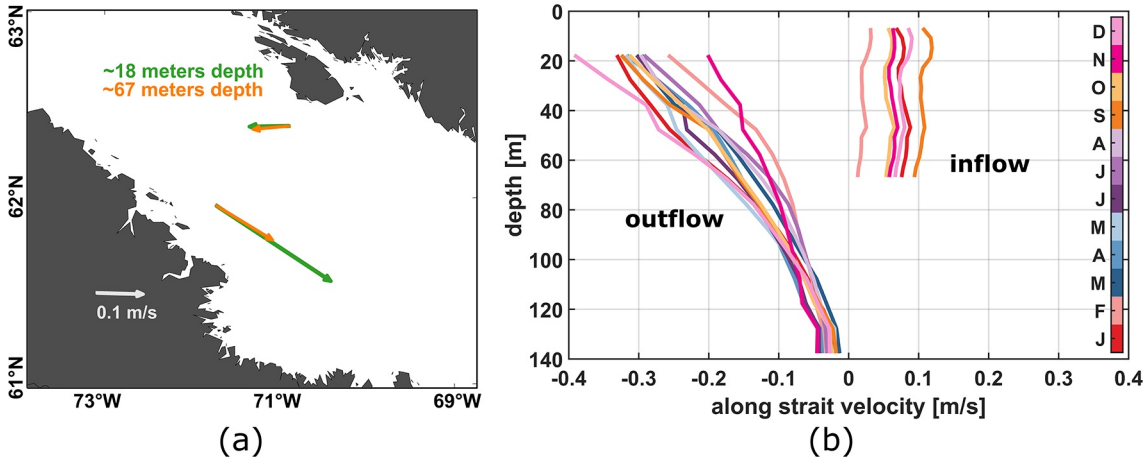

Figure 10. (a) Averaged velocities from August 27, 2008 to March 4, 2009 at roughly 18 and 67 m depth (green and orange respectively) for Moorings A and F. (b) Monthly mean along-strait velocity profiles for the outflow (Mooring A ADCP) and for the inflow (Mooring F ADCP).

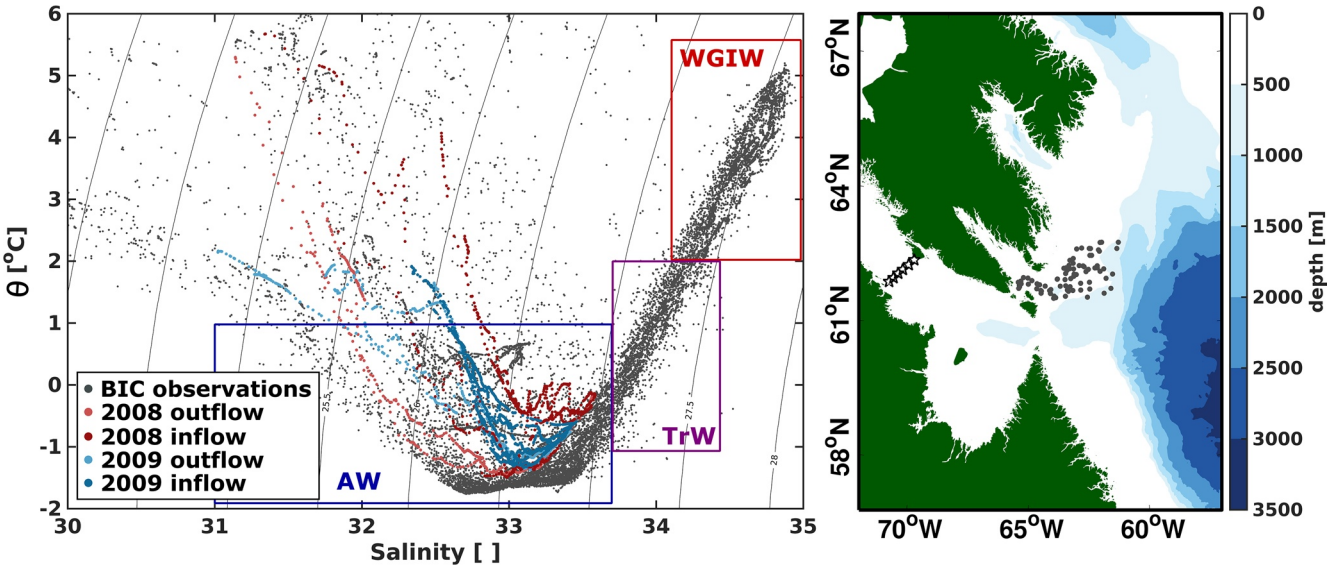

Figure 11. Baffin Island Current (BIC) observations (gray) from August–September 2008 and 2009 (≤ 400 m) with Hudson Strait hydrographic data presented earlier. Red points show data from August 2008 with light points indicating outflow and dark points indicating inflow. Similarly, blue points show data from September 2009. Boxes defining Arctic Water (AW; blue), Transitional Water (TrW; purple), and West Greenland Irminger Water (WGIW; red) are based on definitions defined by Curry et al. (2011). The map shows locations of the BIC observations with gray points, while the stars indicate the hydrographic section in Hudson Strait.

Velocities along the northern side of the strait were weaker throughout the upper 67 m of the water column compared to the outflow. The largest velocities occurred in September, with the weakest flow in February. Our data agree with Drinkwater (1988) in that vertical shear was smaller on the northern side of the strait compared to the southern side, however, vertical velocity shear in their inflow data was still larger, as our inflow exhibited negligible vertical shear. Our inflow velocities at Mooring F contained some component of cross-strait flow, differing from the eastern Hudson Strait section occupied by Drinkwater (1988). The cross-strait flow here is potentially driven by the frontal system described by Cyr and Larouche (2015).

5. Source Waters for Hudson Strait

Using the summer hydrographic survey data with additional property data from the BIC (Section 2.3), we found that the majority of Hudson Strait inflow (and outflow) laid within the Arctic Water (AW) definition (Figure 11; Curry et al., 2011). Hudson Strait inflow waters at mid-depth (salinities around 33) were generally warmer than their BIC AW counterpart during summer. Hudson Strait is an area of intense tidal mixing, and mixing with seasonally warmed surface waters could explain this increase in temperature.

The range of the temperature and salinity measurements in the August 2008 hydrographic occupation was considerably larger than that in September 2009 (Figure 11). This could be because the data was collected in different months (August vs. September) and the differences are a result of the seasonal cycle, or because of differences between 2008 and 2009. To determine the potential cause, we investigated the outflow and inflow separately, using the moored property data to estimate the expected August to September differences. From the moored data, we calculated an average temperature and salinity profile for each August and September 2008 and 2009 for Mooring A and Mooring F. Outflow properties (Mooring A) showed little difference between the two years, with warmer waters in September compared to August. However, when we did a similar comparison of the inflow properties (Mooring F), we found that waters in 2008 were warmer and more saline than those collected in 2009, regardless of month.

To quantify the monthly and yearly changes in the properties of the inflow and outflow data, we calculated the difference in temperature and salinity on the 26.4 isopycnal using the profiles mentioned above. First, we determined the average difference in properties between the inflow and outflow for each year (2008 and

2009). The temperature (salinity) difference between the two flows in 2008 was 0.97°C (0.10). In 2009, the difference between the two flows was less, with a temperature (salinity) difference of 0.26°C (0.01).

To establish what part of this change was due to August-September differences, we took the August–September difference in the outflow (Mooring A) for each year and subtracted these values from the total difference between the two flows (the values mentioned above) for each 2008 and 2009. This isolated the differences in the inflow, and thus we had a measure of how much of the spread is due to the inflow or the outflow. In 2008, we found that 70% (0.68°C) of the temperature difference, and 75% (0.07) of the salinity difference, between the inflow and outflow was due to the inflow properties. In 2009, however, only 24% (0.06°C) of the temperature difference was explained by the inflow, while differences in salinity were explained solely by the variability of the outflow. This suggests that the larger T/S spread in 2008 was mainly due to changes in the inflow properties, which cannot be attributed entirely to the time of the survey but are likely due to interannual changes in the inflow.

6. Hudson Strait Inflow Pathways Within the HBC

One of the other open questions with regards to the Hudson Strait inflow is its fate within the HBC. Once the inflow enters Hudson Strait, part of it is recirculated to the outflow via the cross-strait flow, which is present to as far as Big Island. The remainder however, flows deeper into Hudson Strait (Drinkwater, 1986).

We compared the summer hydrographic data from Hudson Strait to available profiles in western Hudson Strait, Foxe Basin, and northern Hudson Bay (Figure 12) to examine the pathways of the Hudson Strait inflow. As data is sparse in this region, our analysis may provide additional information as to the fate of Hudson Strait inflow waters in the HBC.

Inflowing waters primarily remain along the northern coast in western Hudson Strait (Figure 12, top panel). This result is inconsistent with Dunbar (1951), who found no inflowing waters west of Big Island; this could be due to the sparsity of observations at that time. The properties in northwestern Hudson Strait are similar to those observed in the middle of the strait, indicating little to no water mass modification or mixing along this section of the pathway. Farther west, near Southampton Island, advected and modified Hudson Strait waters appear to form the deep waters in this location (dark gray points in the top panels of Figure 12). This region is the intersection of Foxe Basin, Hudson Bay, and Hudson Strait, and has the potential for complicated flow dynamics.

It is possible that modified inflow waters enter Foxe Basin at middepth, as there is some overlap in the TS properties, which would agree with Defossez et al. (2012). The presence of AW in Foxe Basin from Fury and Hecla Strait makes determining inflow pathways more challenging. Our analysis agrees with earlier studies (Campbell, 1959; Prinsenberg, 1986b) in that modified inflowing waters at mid-depth might be present around Foxe Peninsula (Figure 12, middle panel). Surface and deep waters that are formed in Foxe Basin could contain transformed Hudson Strait waters. Deep waters in Foxe Basin likely remain at depth in Foxe Channel until they overflow the sill (at 180 m) east of Southampton Island (Defossez et al., 2010). Hudson Strait inflow could also potentially enter Foxe Basin near Southampton Island as indicated by Florindo-López et al. (2020, their Figure 5) and Figure 3 by Tao and Myers (2021). However, without velocity data, it is difficult to confirm where these waters are coming from.

The other pathway that Hudson Strait inflow can take is to flow directly into Hudson Bay (Figure 12, bottom panel). Eastern Hudson Bay is cold and fresh along the coast, due to river discharge. Deep waters in northeast Hudson Bay might also have a signal from Hudson Strait (or Foxe Basin) where current reversals have been indicated (Granskog et al., 2011; Prinsenberg, 1986a; St-Laurent et al., 2012). Northwestern Hudson Bay (dark gray points in Figure 12, bottom panel), however, does exhibit evidence of Hudson Strait inflow, in agreement with Florindo-López et al. (2020) and Jones and Anderson (1994). These water masses may have been modified due to mixing at the intersection of Foxe Basin, Hudson Bay, and Hudson Strait, with mixing decreasing with depth. The characteristic "hockey stick" shape of the inflow waters is still intact, though it has shifted to lower salinities. This route is likely the main pathway for Hudson Strait inflow waters inside the HBC.

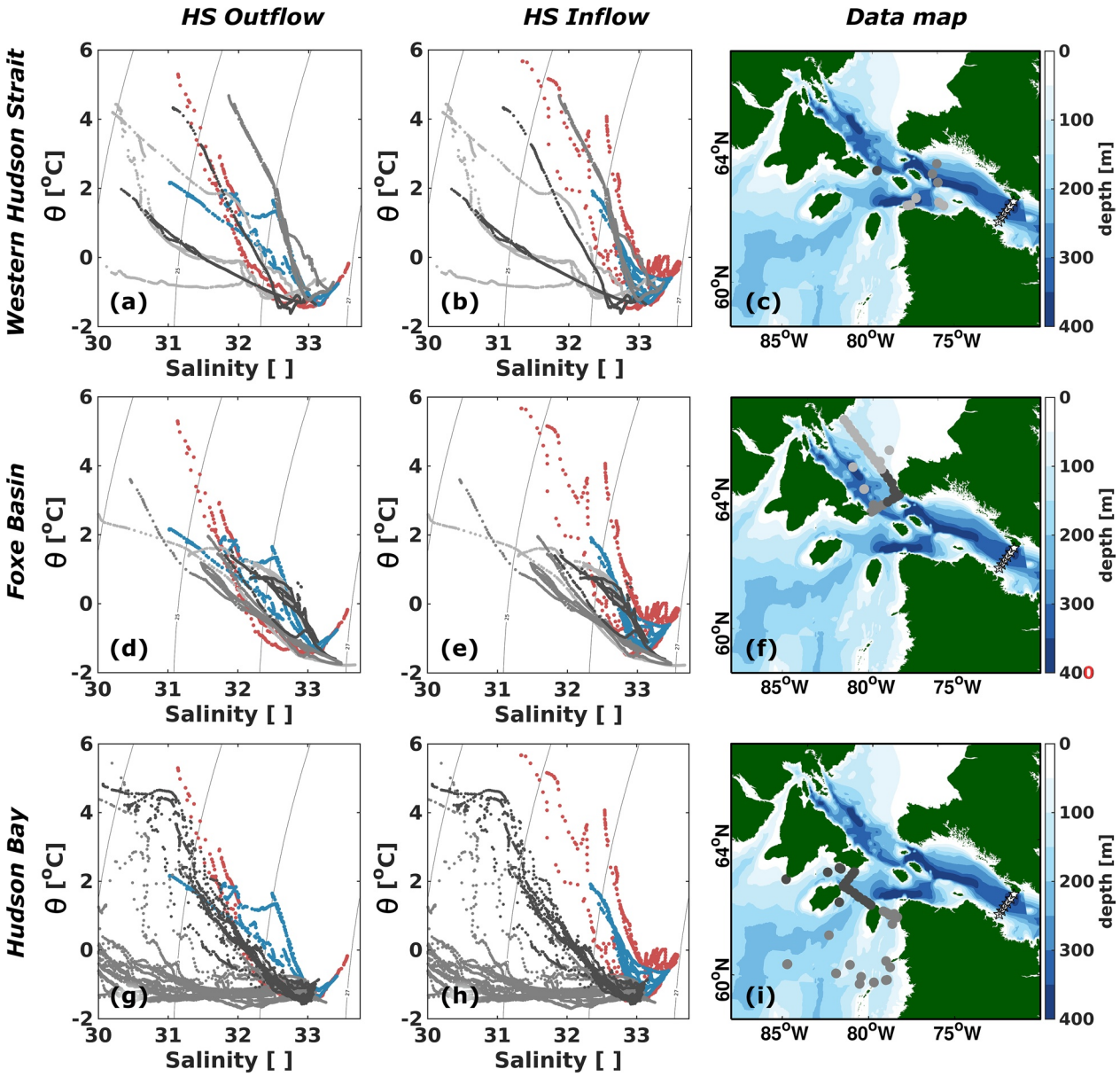

Figure 12. Three regions showing potential pathways of Hudson Strait inflow water; western Hudson Strait (top panels), Foxe Basin (middle panels), and Hudson Bay (bottom panels). Columns show the comparison of Hudson Strait outflow (left) and inflow (center) data with additional data (gray points). Data locations are shown in the corresponding maps (right column). Gray shading indicates different subregions, and correspond to the data shown in the T-S diagrams. Red points show Hudson Strait hydrographic data taken at mid-strait (indicated by stars in the maps), from August 2008, while blue points show data from September 2009.

This result differs from earlier studies as exchange between Hudson Bay and Foxe Basin was thought to occur between Mansel and Southampton Islands with no contribution from Hudson Strait (Drinkwater, 1986; Prinsenberg, 1986a). Additionally, data presented by Jones and Anderson (1994) and Prinsenberg (1986c) did not show the warmer waters at depth from Hudson Strait that we see in our data. Differences are likely due to different seasonal conditions or long-term changes in the circulation.

7. Summary

The HBC is a relatively isolated region, with the only connections to the global ocean being Fury and Hecla Strait to the north and Hudson Strait to the east. As the flow through Fury and Hecla Strait is small, Hudson Strait is the main gateway exchanging waters between the HBC and the global ocean. Hudson Strait exports low salinity water to the Labrador Sea along its southern coast, while importing more saline waters along its northern coast to the HBC. In this study, we presented the first analysis of year-round measurements of the Hudson Strait inflow. This data set is comprised of four moorings across the strait, one on the southern side, and three on the northern side. These data were accompanied by hydrographic data from mooring deployment and recovery cruises in August 2008 and September 2009. Unfortunately instrument failure on the northern moorings limited our ability to estimate transport in the inflow. Nonetheless, we provide a detailed description of the properties of the inflow and examine the origin and pathways of the Hudson Strait inflow.

The inflow, which does not have as fresh of a boundary current feeding it, shows reduced variability throughout the year in both salinity and velocities compared to the outflow. Inflow salinities ranged between 31.3 and 33.8 throughout the year, with a potential density range of 1,024.8–1,027.1 kg m^{-3}. Annual changes in temperature in the inflow were similar at the three northern moorings. We can separate the inflow waters into surface waters, cold intermediate waters, and warmer, saline bottom waters. Inflow waters at the surface underwent a seasonal temperature range of −1.8°C to 4.7°C, while at depth (200 m to bottom) the range was smaller, from −1.8°C to 1.0°C. Salinity of the mid-depth and bottom waters underwent little change throughout the year, from 32.6 to 33.8, while surface waters underwent larger seasonal changes (31.3–33.1).

We determined that the inflow waters are mainly Arctic Waters (AWs), derived from the BIC. The inflow waters transit along the northern side of the strait, with a portion of the inflow entering northern Hudson Bay, with some modification, to become deep waters in the bay. We suspect that some mid-depth Hudson Strait water may also enter Foxe Basin.

The seasonal variability in the inflow velocity did not correlate with the seasonality of the outflow velocities (with the available six months of data shown). There also appeared to be no apparent influence on the inflow from the anticyclonic eddies on the southern side of the strait, as was stated to be an open question by Sutherland et al. (2011). The cross-strait flow was still present at mid-strait, recirculating some water to the outflow. We do find that the Hudson Strait inflow properties are consistent with those from the Davis Strait outflow.

Straneo and Saucier (2008b) estimated that a significant portion of the Davis Strait outflow is recirculated in Hudson Strait and Hudson Bay, before exiting in the Hudson Strait outflow. As the Hudson Strait inflow lies within the classification of AW, and would contain a large amount of the freshwater exiting Davis Strait, any anomalous freshwater events passing through Davis Strait could be rerouted in Hudson Strait, and delay the arrival of the anomaly farther downstream.

Previous estimates of the freshwater transport of the inflow (with limited data) were around 41 mSv (Straneo & Saucier, 2008a), using an estimated inflow salinity of 33.1, which we have confirmed with our transport-weighted salinity estimate. However, since 2008, more recent Davis Strait data has been presented (Curry et al., 2014), which may change the ratio between the Davis Strait outflow and Hudson Strait inflow, specifically the proportion of AW entering Hudson Strait.

From Curry et al. (2014), the 2004–2010 mean southward volume transport is −2.9 Sv, which can be separated into −1.8 Sv for AW, and −1.1 Sv for Transitional Water (TrW). Additionally, the southward freshwater transport (referenced to 34.8) is −117 mSv, with AW contributing −98 mSv and TrW contributing −19 mSv (Curry et al., 2014). Earlier work estimated the volume of Hudson Strait inflow to be approximately 0.85 Sv (Drinkwater, 1988). Using the transports from Table 2, and reducing both the volume and freshwater transports by a factor to achieve an inflow volume transport of 0.85 Sv, we get an inflow freshwater transport of about 40 mSv (referenced to 34.8). Maximum transports of AW (volume and freshwater) through Davis Strait occur in October and November (Curry et al., 2014), implying that any significant changes in the ratio of volume and freshwater would occur after the hydrographic sections were taken. We find that the inflow is AW from the BIC, which means that about 47% of AW, or 1/3 of the southward volume transport (agreeing with Straneo & Saucier, 2008b), from Davis Strait enters Hudson Strait. As for freshwater, this implies that

34% of the southward freshwater transport (similar to Straneo & Saucier, 2008b), or about 40% of AW freshwater, from Davis Strait enters Hudson Strait. This confirms the notion that the HBC may modify a sizable fraction of any AW anomaly emerging from Davis Strait before it reaches the Labrador Sea.

These data can help validate, and be complemented by, numerical simulations. Continued observational efforts, however, are still needed in the strait to understand the impact that large-scale changes presently occurring in the Arctic Ocean and atmosphere may have on the variability in the Hudson Strait inflow and therefore the HBC.

The HBC system is currently experiencing, and expected to further undergo, rapid change, consistent with the changes occurring in the sea ice-covered regions in the Arctic, such as the Barents Sea (Onarheim & Årthun, 2017). Until now, however, there had been no baseline measurements to compare future changes to. The Hudson Strait inflow is the largest source of oceanic water to the HBC. From this study, we know how the properties of this AW from the BIC vary throughout the year, and we know that a portion of this water enters Hudson Bay. This work provides a baseline on which future work can be compared to and will also help to determine water transformations that occur in this region, as it is the foundation on which the ecosystem and the local people depend.

Appendix A: Calculating Geostrophic Velocities

Geostrophic velocities for each hydrographic section (Figure 4) were calculated using the Gibbs SeaWater Oceanographic Toolbox of TEOS-10. Gridded conservative temperature, absolute salinity, and absolute pressure data are used to calculate the geostrophic stream function, which involves the difference in velocity between the pressure, P, and the reference pressure. The geostrophic velocities were then calculated using the geostrophic stream function relative to the surface pressure.

Calculated geostrophic velocities were referenced to spline interpolated averaged August–September velocities at 100 m. To obtain the reference velocities at 100 m for Mooring A, we linearly interpolated the average August to September velocity profile for each year. On the northern side of the strait, surface velocities at Mooring F are only available until March 2009. We used the mean August to September velocities for each year at Moorings E and G to linearly interpolate a deep velocity value at Mooring F. The average August–September 2008 velocity profile at Mooring F was then linearly interpolated in the vertical to obtain a reference velocity value at 100 m for both 2008 and 2009. We assume that inflow velocities in the top 67 m are horizontally homogeneous across Moorings E, F, and G. Using the average 2008 August to September Mooring F velocity profile in the top 67 m for both Moorings E and G, we linearly interpolated to the mean August to September velocities at these moorings for each year to obtain reference velocities at 100 m for each mooring.

The resulting four reference velocities for each year, were spline interpolated horizontally across the strait. Calculated geostrophic velocities were referenced at 100 m, and then adjusted for net −0.1 Sv volume transport, so as to constrain the outflow. Adjusting for a net −0.1 Sv volume transport, a value, x, was added or subtracted to the velocities before being multiplied by the vertical and horizontal grid. The value, x, was unique to each section. For the 2008 section, $x = -0.0205$, and for the 2009 section, $x = -0.003765$.

Data Availability Statement

The data described in this study can be found at the Arctic Data Center (Straneo, 2021a, 2021b, 2021c). Mooring temperature, salinity, and pressure data can also be found as the National Oceanic and Atmospheric Administration National Centers for Environmental Information (NOAA NCEI) and are cited as Straneo (2014).

Acknowledgments
First, the authors would like to thank two anonymous reviewers for their constructive feedback which helped to clarify and improve the manuscript. The authors would like to thank the captains and crews of the RV Knorr (cruise numbers 194-01 and 196-01). Support from NSERC (RGPIN 04357, awarded to PGM) to fund a research stay for NAR at Scripps Institution of Oceanography made this work possible. FS and JH acknowledge support from NSF OCE 1756272. The authors thank ArcticNet for funding and instruments for Moorings E and G. The authors appreciate the use of the AMSR-E sea ice concentration data as well as the additional temperature and salinity data from the World Ocean Database and the Oceanography and Scientific Data-Marine Environmental Data Service.

References

Amante, C., & Eakins, B. (2009). *ETOPO1 1 Arc-Minute Global Relief Model: Procedures, Data Sources and Analysis. NOAA Technical Memorandum NESDIS NGDC-24*. National Geophysical Data Center, NOAA. https://doi.org/10.7289/V5C8276M

Arbic, B. K., St-Laurent, P., Sutherland, G., & Garrett, C. (2007). On the resonance and influence of the tides in Ungava Bay and Hudson Strait. *Geophysical Research Letters*, *34*(17), L17606. https://doi.org/10.1029/2007GL030845

Babb, D., Andrews, J., Dawson, J., Landry, D., Mussells, O., & Weber, M. (2019). Transportation and community use of the marine environment. In Z. Kuzyk, & L. E. L. M. Candlish (Eds.), *From science to policy in the Greater Hudson Bay Marine Region: An Integrated Regional Impact Study (IRIS) of climate change and modernization* (pp. 341–377).

Bakker, P., Schmittner, A., Lenaerts, J. T. M., Abe-Ouchi, A., Bi, D., van den Broeke, M. R., et al. (2016). Fate of the Atlantic Meridional Overturning Circulation: Strong decline under continued warming and Greenland melting. *Geophysical Research Letters*, *43*(23), 12252–12260. https://doi.org/10.1002/2016GL070457

Bamber, J. L., Tedstone, A. J., King, M. D., Howat, I. M., Enderlin, E. M., van den Broeke, M. R., et al. (2018). Land ice freshwater budget of the Arctic and North Atlantic Oceans: 1. Data, methods, and results. *Journal of Geophysical Research: Oceans*, *123*(3), 1827–1837. https://doi.org/10.1002/2017JC013605

Barber, F. G. (1965). Current observations in Fury and Hecla Strait. *Journal of the Fisheries Research Board of Canada*, *22*(1), 225–229. https://doi.org/10.1139/f65-021

Böning, C. W., Behrens, E., Biastoch, A., Getzlaff, K., & Bamber, J. L. (2016). Emerging impact of Greenland meltwater on deepwater formation in the North Atlantic Ocean. *Nature Geoscience*, *9*, 523–527. https://doi.org/10.1038/ngeo2740

Boyer, T., Baranova, O. K., Coleman, C., Garcia, H. E., Grodsky, A., Locarnini, R. A., et al. (2018). *World Ocean Database 2018*.

Campbell, N. (1959). *Some oceanographic features of northern Hudson Bay, Foxe Channel, and Hudson Strait (Tech. Rep. No. 46)*. Fisheries Research Board of Canada.

Candlish, L., Babb, D., Andrews, J., Myers, P., Ridenour, N., Landy, J., & Ehn, J. (2019). Characteristics of the seasonal sea ice cover. In Z. Kuzyk, & L. E. L. M. Candlish (Eds.), *From science to policy in the Greater Hudson Bay Marine Region: An Integrated Regional Impact Study (IRIS) of climate change and modernization* (pp. 79–95).

Castro de la Guardia, L., Myers, P. G., Derocher, A. E., Lunn, N. J., & Terwisscha van Scheltinga, A. D. (2017). Sea ice cycle in western Hudson Bay, Canada, from a polar bear perspective. *Marine Ecology Progress Series*, *564*, 225–233. https://doi.org/10.3354/meps11964

Curry, B., Lee, C. M., & Petrie, B. (2011). Volume, freshwater, and heat fluxes through Davis Strait, 2004–05. *Journal of Physical Oceanography*, *41*(3), 429–436. https://doi.org/10.1175/2010JPO4536.1

Curry, B., Lee, C. M., Petrie, B., Moritz, R. E., & Kwok, R. (2014). Multiyear volume, liquid freshwater, and sea ice transports through Davis Strait, 2004–10. *Journal of Physical Oceanography*, *44*(4), 1244–1266. https://doi.org/10.1175/JPO-D-13-0177.1

Cyr, F., Bourgault, D., & Galbraith, P. S. (2011). Interior versus boundary mixing of a cold intermediate layer. *Journal of Geophysical Research: Oceans*, *116*(C12), C12029. https://doi.org/10.1029/2011JC007359

Cyr, F., & Larouche, P. (2015). Thermal fronts Atlas of Canadian coastal waters. *Atmosphere-Ocean*, *53*(2), 212–236. https://doi.org/10.1080/07055900.2014.986710

Defossez, M., Saucier, F., Myers, P., Caya, D., & Dumais, J. (2012). Comparing winter and summer simulated Estuarine circulations in Foxe Basin, Canada. *Atmosphere-Ocean*, *50*(3), 386–401. https://doi.org/10.1080/07055900.2012.693256

Defossez, M., Saucier, F., Myers, P., Caya, D., & Dumais, J.-F. (2010). Analysis of a dense water pulse following mid-winter opening of polynyas in western Foxe Basin, Canada. *Dynamics of Atmospheres and Oceans*, *49*, 54–74. https://doi.org/10.1016/j.dynatmoce.2008.12.002

Déry, S. J., Stieglitz, M., McKenna, E. C., & Wood, E. F. (2005). Characteristics and trends of river discharge into Hudson, James, and Ungava Bays, 1964–2000. *Journal of Climate*, *18*(14), 2540–2557. https://doi.org/10.1175/jcli3440.1

Drinkwater, K. (1986). Chapter 13 Physical Oceanography of Hudson Strait and Ungava Bay. *Elsevier Oceanography Series*, *44*, 237–264. (Canadian Inland Seas). https://doi.org/10.1016/s0422-9894(08)70906-1

Drinkwater, K. (1988). On the mean and tidal currents in Hudson Strait. *Atmosphere-Ocean*, *26*(2), 252–266. https://doi.org/10.1080/07055900.1988.9649302

Dunbar, M. (1951). *Eastern Arctic Waters (Tech. Rep. No. 88)*. Fisheries Research Board of Canada.

Finlay, C. C., Maus, S., Beggan, C. D., Hamoudi, M., Lowes, F. J., Olsen, N., & Thébault, E. (2010). Evaluation of candidate geomagnetic field models for IGRF-11. *Earth, Planets and Space*, *62*(8), 787–804. https://doi.org/10.5047/eps.2010.11.005

Florindo-López, C., Bacon, S., Aksenov, Y., Chafik, L., Colbourne, E., & Holliday, N. P. (2020). Arctic Ocean and Hudson Bay freshwater exports: New estimates from 7 Decades of hydrographic surveys on the Labrador Shelf. *Journal of Climate*, *33*, 8849–8868. https://doi.org/10.1175/JCLI-D-19-0083.1

Foreman, M. G. G., Crawford, W. R., Cherniawsky, J. Y., Gower, J. F. R., Cuypers, L., & Ballantyne, V. A. (1998). Tidal correction of TOPEX/POSEIDON altimetry for seasonal sea surface elevation and current determination off the Pacific coast of Canada. *Journal of Geophysical Research: Oceans*, *103*(C12), 27979–27998. https://doi.org/10.1029/98JC02671

Granskog, M. A., Kuzyk, Z. Z. A., Azetsu-Scott, K., & Macdonald, R. W. (2011). Distributions of runoff, sea-ice melt and brine using $\delta^{18}O$ and salinity data—A new view on freshwater cycling in Hudson Bay. *Journal of Marine Systems*, *88*, 362–374. (The Hudson Bay System). https://doi.org/10.1016/j.jmarsys.2011.03.011

Haine, T. W., Curry, B., Gerdes, R., Hansen, E., Karcher, M., Lee, C., et al. (2015). Arctic freshwater export: Status, mechanisms, and prospects. *Global and Planetary Change*, *125*, 13–35. https://doi.org/10.1016/j.gloplacha.2014.11.013

Hochheim, K. P., & Barber, D. G. (2014). An update on the ice climatology of the Hudson Bay system. *Arctic, Antarctic, and Alpine Research*, *46*(1), 66–83. https://doi.org/10.1657/1938-4246-46.1.66

Jones, E. P., & Anderson, L. G. (1994). Northern Hudson Bay and Foxe Basin: Water masses, circulation and productivity. *Atmosphere-Ocean*, *32*(2), 361–374. https://doi.org/10.1080/07055900.1994.9649502

Lazier, J. R. (1980). Oceanographic conditions at Ocean Weather Ship Bravo, 1964–1974. *Atmosphere-Ocean*, *18*(3), 227–238. https://doi.org/10.1080/07055900.1980.9649089

LeBlond, P. H., Osborn, T., Hodgins, D., Goodman, R., & Metge, M. (1981). Surface circulation in the western Labrador Sea. *Deep Sea Research Part A. Oceanographic Research Papers*, *28*(7), 683–693. https://doi.org/10.1016/0198-0149(81)90129-1

Loder, J., Petrie, B., & Gawarkiewicz, G. (1998). The coastal ocean off northeastern North America: A large-scale view. In *The Sea* (Vol. 11, p. 105–133). John Wiley & Sons

Marsden, R., & Gratton, Y. (1998). Surface pulses in the lower St. Lawrence Estuary. *Atmosphere-Ocean*, *36*(3), 271–295. https://doi.org/10.1080/07055900.1998.9649614

Onarheim, I. H., & Årthun, M. (2017). Toward an ice-free Barents Sea. *Geophysical Research Letters*, *44*(16), 8387–8395. https://doi.org/10.1002/2017GL074304

O'Reilly, C. T., Solvason, R., & Solomon, C. (2005). Where are the world's largest tides? In J. Ryan (Ed.), *BIO Annual Report "2004 in review"* (pp. 44–46).

Pawlowicz, R., Beardsley, B., & Lentz, S. (2002). Classical tidal harmonic analysis including error estimates in MATLAB using T_TIDE. *Computers & Geosciences*, *28*(8), 929–937. https://doi.org/10.1016/S0098-3004(02)00013-4

Petrie, B., Akenhead, S., Lazier, J., & Loder, J. (1988). *The cold intermediate layer on the Labrador and northeast Newfoundland Shelves 1978–1986*.

Prinsenberg, S. (1986a). Chapter 10 the circulation pattern and current structure of Hudson Bay. *Elsevier Oceanography Series*, *44*, 187–204. https://doi.org/10.1016/S0422-9894(08)70903-6

Prinsenberg, S. (1986b). Chapter 12 on the physical oceanography of Foxe Basin. *Elsevier Oceanography Series*, *44*, 217–236. (Canadian Inland Seas). https://doi.org/10.1016/s0422-9894(08)70905-x

Prinsenberg, S. (1986c). Chapter 9 salinity and temperature distributions of Hudson Bay and James Bay. *Elsevier Oceanography Series*, *44*, 163–186. https://doi.org/10.1016/S0422-9894(08)70902-4

Ramsey, A. L., & Straneo, F. (2018). *Pathways for the export of Arctic change into the North Atlantic August 2008 to September 2009 Data Report (Tech. Rep.)*. Woods Hole Oceanographic Institution. https://doi.org/10.1575/1912/9575

Ridenour, N. A., Hu, X., Jafarikhasragh, S., Landy, J. C., Lukovich, J. V., Stadnyk, T. A., et al. (2019). Sensitivity of freshwater dynamics to ocean model resolution and river discharge forcing in the Hudson Bay Complex. *Journal of Marine Systems*, *196*, 48–64. https://doi.org/10.1016/j.jmarsys.2019.04.002

Sadler, H. E. (1982). Water flow into Foxe Basin through Fury and Hecla Strait. *Naturaliste Canadien*, 701–707.

Saucier, F., Larouche, P., D'Astous, A., & Dionne, J. (1994). Moored physical oceanographic data from northeastern Hudson Bay between August 1992 and September 1993. *Canadian Data Report of Hydrography and Ocean Sciences*, *132*, 73.

Saucier, F. J., Senneville, S., Prinsenberg, S., Roy, F., Smith, G., Gachon, P., et al. (2004). Modeling the sea ice-ocean seasonal cycle in Hudson Bay, Foxe Basin and Hudson Strait, Canada. *Climate Dynamics*, *23*(3/4), 303–326. https://doi.org/10.1007/s00382-004-0445-6

Spreen, G., Kaleschke, L., & Heygster, G. (2008). Sea ice remote sensing using AMSR-E 89-GHz channels. *Journal of Geophysical Research: Oceans*, *113*(C2), C02S03. https://doi.org/10.1029/2005JC003384

St-Laurent, P., Straneo, F., & Barber, D. G. (2012). A conceptual model of an Arctic sea. *Journal of Geophysical Research: Oceans*, *117*(C6), C06010. https://doi.org/10.1029/2011JC007652

St-Laurent, P., Straneo, F., Dumais, J.-F., & Barber, D. (2011). What is the fate of the river waters of Hudson Bay? *Journal of Marine Systems*, *88*, 352–361. (The Hudson Bay System). https://doi.org/10.1016/j.jmarsys.2011.02.004

Straneo, F. (2014). *Temperature, salinity, conductivity and pressure data collected from a moored buoy in Hudson Strait from 2008-08 to 2009-09 (NCEI accession 0119894)*. Retrieved from https://accession.nodc.noaa.gov/0119894

Straneo, F. (2021a). *Moored velocity measurements in Hudson Strait from August 2008 to September 2009*. https://doi.org/10.18739/A2F18SG3T

Straneo, F. (2021b). *Profiles of temperature, salinity, and beam transmission, and bathymetry data, from Hudson Strait from September 25–26, 2009*. https://doi.org/10.18739/A29882P0J

Straneo, F. (2021c). *Profiles of temperature, salinity, dissolved oxygen, and fluorescence from Hudson Strait from August 26, 2008*. https://doi.org/10.18739/A2JS9H865

Straneo, F., & Saucier, F. (2008b). The outflow from Hudson Strait and its contribution to the Labrador Current. *Deep Sea Research Part I: Oceanographic Research Papers*, *55*(8), 926–946. https://doi.org/10.1016/j.dsr.2008.03.012

Straneo, F., & Saucier, F. J. (2008a). The Arctic-Subarctic exchange through Hudson Strait. In R. R. Dickson, J. Meincke, & P. Rhines (Eds.), *Arctic-Subarctic Ocean Fluxes: Defining the role of the northern seas in climate* (pp. 249–261). Dordrecht: Springer Netherlands. https://doi.org/10.1007/978-1-4020-6774-7_11

Sutherland, D. A., Straneo, F., Lentz, S. J., & Saint-Laurent, P. (2011). Observations of fresh, anticyclonic eddies in the Hudson Strait outflow. *Journal of Marine Systems*, *88*, 375–384.(The Hudson Bay System) . https://doi.org/10.1016/j.jmarsys.2010.12.004

Tao, R., & Myers, P. G. (2021). Modeling the advection of pollutants in the Hudson Bay complex. *Journal of Marine Systems*, *214*, 103474. https://doi.org/10.1016/j.jmarsys.2020.103474

Yang, Q., Dixon, T. H., Myers, P. G., Bonin, J., Chambers, D., van den Broeke, M. R., et al. (2016). Recent increases in Arctic freshwater flux affects Labrador Sea convection and Atlantic overturning circulation. *Nature Communications*, *7*(1), 10525. https://doi.org/10.1038/ncomms10525